Effect of Vinylene Carbonate Additive in Li-Ion Batteries: Comparison of LiCoO2/C, LiFePO4/C, and LiCoO2/Li4Ti5O12 Systems

L. El Ouatani, Rémi Dedryvère, C. Siret, P. Biensan, D. Gonbeau

The effect of Vinylene Carbonate additive in Li-ion batteries: comparison of $LiCoO_2$/C, $LiFePO_4$/C and $LiCoO_2$/$Li_4Ti_5O_{12}$ systems

L. El Ouatani,[a] R. Dedryvère,[a,z] C. Siret,[b] P. Biensan,[b] D. Gonbeau[a]

[a] *IPREM, University of Pau, 64053 Pau cedex 9, France*

[b] *SAFT, 33074 Bordeaux cedex, France*

Abstract

Vinylene Carbonate (VC) is a commonly used electrolyte additive in Li-ion batteries, because of its beneficial role on the formation of the solid electrolyte interphase (SEI). It was shown to contribute to surface film formation on both electrodes of $LiCoO_2$/C cells via its radical polymerization mechanism. In this paper, we carried out a comparative study of the role of VC on electrode/electrolyte interfaces in $LiCoO_2$/C, $LiFePO_4$/C and $LiCoO_2$/$Li_4Ti_5O_{12}$ systems, in which the potential and the chemical nature of each electrode are changed. Coin-cells were charged at different potentials using a $LiPF_6$/EC:DEC:DMC liquid electrolyte with or without VC, and the electrodes were analyzed by X-ray Photoelectron Spectroscopy (XPS). We showed there is no interaction between the negative and the positive electrode in the VC polymerization mechanisms – for example by exchange of chemical species from one electrode to the other one – during the first charge. Separate mechanisms occur, although the same VC polymer is deposited at the surface of both electrodes.

Keywords: Li-ion batteries, XPS, interface, SEI, polymerization, vinylene carbonate, electrolyte additive, $Li_4Ti_5O_{12}$, $LiFePO_4$.

[z] corresponding author (remi.dedryvere@univ-pau.fr)

1. INTRODUCTION

Most of today's commercial lithium-ion batteries consist of a graphitic carbon anode, a layered transition metal oxide cathode ($LiCoO_2$), and a nonaqueous organic electrolyte based on a solution of a lithium salt ($LiPF_6$) in a mixture of linear and cyclic carbonates. It is well known that a film called Solid Electrolyte Interphase (SEI) is formed at the surface of the graphite negative electrode during the first cycles. It is generally admitted that the SEI layer originates from the reductive decomposition of the electrolyte solvents and salt on the negative electrode, making up a protective film that prevents side reactions (such as solvent cointercalation into graphite) and further decomposition of the electrolyte components. The chemical nature and morphology of this film play an important role in cycle life, power capability and safety of the battery [1-4]. Much less studies have been devoted to the film formed at the surface of the positive electrode, but it is now demonstrated that it also plays an important role in the battery performances [5-8]. Many research studies are thus focused on the improvement of the electrolyte. The use of electrolyte additives is an efficient method to improve the SEI properties [9,10]. The most used electrolyte additive is vinylene carbonate (VC). It was early proposed by SAFT [11] and was the subject of numerous studies [12-28]. The main advantage of VC is its preferential reduction, prior to other electrolyte solvents, which results in a better SEI on the negative electrode. It was shown using C/Li half-cells that the presence of VC as additive in the electrolyte results in a higher reversible capacity of the graphite electrode, and an improved cycle life and performance at elevated temperature [12,13,19,23,25,26]. For $LiCoO_2$/C cells, VC improves the cycling behavior and reduces the cell impedance. The positive effects of VC are mainly attributed to reactions at the graphite negative electrode. Nevertheless some studies have shown that VC may have some effect on the positive electrode [15,17,20,28-32]. The influence of VC on other systems ($LiFePO_4$/graphite, $LiCoO_2/Li_4Ti_5O_{12}$) was also investigated [33,34]. Wu *et al.* reported that

the addition of VC in the electrolyte improves the high-temperature cycling performance of $LiFePO_4$/C batteries. They showed that VC modifies the $LiFePO_4$ electrode/electrolyte interface, and suppresses iron dissolution and its subsequent deposition on the negative electrode side.

While the beneficial role of VC on electrode/electrolyte interfaces has been demonstrated, the exact reaction mechanisms at the surface of the electrodes are still not completely understood. In a first paper [35], we studied the degradation mechanisms of VC that lead to surface film formation on both electrodes in a $LiCoO_2$/graphite cell. We showed that the main solid compound deposited at the surface of both electrodes is a polymer ensuing from the radical polymerization of VC, which consists of a repetition of EC (ethylene carbonate) rings, as shown in Scheme 1. In this first paper [35], we carried out the X-ray Photoelectron Spectroscopy (XPS) investigation of $LiCoO_2$/graphite coin-cells using a $LiPF_6$/EC:DEC:DMC liquid electrolyte with and without VC additive, completed by *ab initio* calculations and direct synthesis of the VC polymer formed at the surface of the electrodes. We showed that the presence of this polymer at the surface of the electrodes can be characterized by the presence, in XPS spectra, of two O 1s peaks at 533 and 534.5 eV. The second one corresponds to a very high binding energy (534.5 eV), and only a few oxygenated organic species can reach such a high binding energy value. We showed that this particular peak could be used as a signature of this VC polymer, and that its intensity increases upon charge of the $LiCoO_2$/graphite cell [35]. As shown in Figure 1, this peak was observed only when VC was added in the electrolyte, and its intensity increased when an electrolyte made up of $LiPF_6$ dissolved in pure VC was used.

Despite these new results, many fundamental questions still remain open about the exact role of VC on surface film formation in Li-ion batteries. For example, whereas it is now clear that both $LiCoO_2$ and graphite electrodes are simultaneously covered by the same VC

polymer, the question of a possible interaction between both electrodes in the polymerization mechanism is not resolved. Indeed, the formation of these surface films may result either from two independent degradation mechanisms of VC leading to the same final product, or from a joint mechanism involving both electrodes. Whereas some authors have already proposed reduction mechanisms of VC into a radical anion at the surface of graphite [36] that could explain to the radical polymerization of VC at the negative electrode, to our knowledge no equivalent oxidation mechanism of VC into radical cations at the positive electrode has been proposed.

The aim of the present paper is to investigate the possible interaction between both electrodes in the polymerization mechanism of VC. With this aim, we embarked on a comparative study of $LiFePO_4$/C and $LiCoO_2$/$Li_4Ti_5O_{12}$ systems with respect to $LiCoO_2$/C. In this approach, we investigated the influence of the potential of each electrode and its chemical nature on the formation of the surface films upon charge when VC is added in the electrolyte. The electrochemical charge of these systems has been carried out in coin-cells using a $LiPF_6$/EC:DEC:DMC electrolyte, with or without VC additive. Graphite/Li half-cells have been also investigated. The electrode/electrolyte interfaces have been analyzed by XPS at different potentials of the first charge or discharge.

2. EXPERIMENTAL SECTION

2.1. Electrochemical measurements: The electrode materials were provided by SAFT. The graphite electrodes consisted of a mixture of graphite, SBR (Styrene Butadiene Rubber) and CMC (carboxymethylcellulose sodium salt) as binders, deposited on a copper foil current collector. The $LiCoO_2$, $LiFePO_4$, and $Li_4Ti_5O_{12}$ electrodes were prepared by coating an aluminum foil current collector with a slurry of active material powder, conductive carbon and poly(vinylidene fluoride) PVdF binder, in *N*-methyl-2-pyrrolidone. The electrodes were

then dried at 120°C for 12 h in an oven. For graphite/Li half-cells, a metallic lithium foil was used as negative electrode. Two kinds of electrolytes were used: *(a)* $LiPF_6$ 1mol/L in EC:DEC:DMC (2:1:2 in volume ratio) and *(b)* the same with a few percent of VC additive. The purity of the salt $LiPF_6$ was 99.98 wt.% min (water ≤ 20 ppm). The purity of solvents EC, DEC and DMC was 99.98 wt.% min (water ≤ 20 ppm, methanol + ethanol ≤ 50 ppm). The purity of VC was 99.9 wt.% (water ≤ 40 ppm, sulfate 50 ppm, chloride 2 ppm). As usually, this commercial VC contained the stabilizer BHT (2,6-di-tBu-4-methylphenol).

Graphite/Li, $LiFePO_4$/graphite and $LiCoO_2/Li_4Ti_5O_{12}$ coin-cells were assembled in a Jacomex argon dry box, in which the oxygen and water contents were maintained below 2 ppm, and then charged (or discharged for C/Li half-cells) at 20°C using a Multichannel Potentiostat Galvanostat MPG testing apparatus (Bio-Logic SAS, Claix, France) performing under galvanostatic mode at C/20 rate (*i.e.* the full charge – or discharge – capacity of the cell is reached in 20 hours). Then, the electrodes were carefully separated from the rest of the battery components in an argon dry box, washed with DMC solvent to remove the electrolyte, and dried prior to being packed into a hermetically sealed aluminum bag for transportation.

2.2. XPS: XPS measurements were carried out with a Kratos Axis Ultra spectrometer, using a focused monochromatized Al Kα radiation (hν = 1486.6 eV). The XPS spectrometer was directly connected through a transfer chamber to a dry box, in order to avoid moisture/air exposure of the samples. For the Ag $3d_{5/2}$ line the full width at half maximum (FWHM) was 0.58 eV under the recording conditions. The analyzed area of the samples was 300 × 700 μm^2. Peaks were recorded with a constant pass energy of 20 eV. The pressure in the analysis chamber was around 5.10^{-7} Pa. Short acquisition time spectra were recorded before and after each normal experiment to check that the samples did not suffer from degradation during the measurements. The binding energy scale was calibrated from the hydrocarbon contamination

using the C 1s peak at 285.0 eV. Core peaks were analyzed using a nonlinear Shirley-type background [37]. The peak positions and areas were optimized by a weighted least-square fitting method using 70 % Gaussian, 30 % Lorentzian lineshapes. Quantification was performed on the basis of Scofield's relative sensitivity factors [38].

3. RESULTS AND DISCUSSION

Figure 2 shows the galvanostatic charge (or discharge) curves of the different systems studied in this work: $LiCoO_2/Li_4Ti_5O_{12}$, $LiFePO_4$/graphite and graphite/Li. The points show the various samples studied ex-situ by XPS. In order to investigate the possible interaction between the positive and the negative electrodes in the formation mechanism of the SEI when VC is added in the electrolyte, we first carried out a comparative study of graphite/Li half-cells with respect to the $LiCoO_2$/graphite system.

3.1. Graphite/Lithium system:

The first electrochemical discharge of the C/Li half-cells at 20°C was stopped at the following potentials: 1.0, 0.2, 0.15 and 0.01 V, using two different electrolytes: *(a)* $LiPF_6$ 1mol/L in EC:DEC:DMC (VC-free), *(b)* the same with a few percent of VC additive. After discharge, each electrode was analyzed by XPS.

Figure 3 shows the evolution of C 1s and O 1s core peaks of the composite graphite electrode upon the first discharge.

C 1s core peak: The C 1s spectrum of the fresh composite electrode consists of five peaks. The first one at 284.3 eV corresponds to graphite. The second one at 285.0 eV is assigned to SBR binder (and also to hydrocarbon contamination), while the two other peaks observed at 286.7 and 288.4 eV are attributed to CO- and CO_2-like carbon atoms in the CMC binder, respectively. Finally, the last weak peak at 291-292 eV is the "shake-up" satellite of graphite due to multielectronic transitions involving π-π^* transitions [39].

For both series of samples, we can observe upon discharge an important decrease of the graphite component at 284.3 eV, showing that the active electrode material has been covered by a SEI film. For both series of samples the graphite component has totally disappeared at 0.2 V, which means that the SEI thickness is greater than the analysis depth of XPS (about 5-10 nm). In the same time, we can observe the appearance of new peaks at 290-290.5 eV attributed to CO_3-like carbon atoms, *i.e.* to carbonate species. This is in good agreement with the deposition of carbonate salts (Li_2CO_3 and/or lithium alkyl carbonates $ROCO_2Li$) at the surface of the electrode, resulting from the decomposition of the solvents EC, DEC and DMC. Several formation mechanisms of these carbonate species can be found in the literature [6,40,41]. They were extensively characterized by XPS in a previous work [42]. When VC is added in the electrolyte, it is worth noting that an additional weak peak at 291.3 eV can be observed at the end of discharge (figure 3*b*). This can be attributed to the deposition of the VC polymer at the surface of the graphite electrode, as shown in our previous work [35]. Overall, the same evolution of the graphite electrode surface was observed upon charge of complete $LiCoO_2$/graphite cells. The main difference here concerns the amount of carbonate species coming from the degradation of the solvents. Indeed, the amount of carbonates observed on the graphite electrode surface is greater in graphite/Li half-cells than in $LiCoO_2$/graphite complete cells.

O 1s core peak: The O 1s spectrum of the composite electrode consists of two peaks assigned to the oxygen atoms of the CMC binder. For both series, we can observe from the beginning of discharge the replacement of the O 1s components attributed to the CMC binder by new components, which show the deposition of new oxygenated species.

When using the VC-free electrolyte (series *a*), the O 1s spectrum after discharge consists of two peaks with a maximum at ~532 eV and a shoulder at ~533.8 eV, which is in good agreement with the deposition of carbonate salts at the surface of the electrode (Li_2CO_3 and/or

lithium alkyl carbonates $ROCO_2Li$), resulting from the decomposition of the solvents, as said above. However, other oxygen-containing compounds may be also present in the SEI.

When using the VC-containing electrolyte (series *b*), the shape of the O 1s spectra is rather different, and a third peak at a high binding energy (534.5 eV) appears. As explained above and shown in our previous work [35], only a few oxygenated organic species can reach such a high O 1s binding energy value, and this particular peak can be considered as a signature of the VC polymer at the surface of the electrodes. The intensity of this peak increases upon discharge, showing the particular formation mechanism of the SEI at the surface of the graphite electrode when VC additive is present.

This is a first important result: despite some small differences (*i.e.* the amount of carbonate compounds ensuing from degradation of the solvents EC, DEC and DMC), the same specific polymerization mechanism of VC which contributes to the formation of the SEI at the surface of the graphite electrode is observed in both graphite/Li and $LiCoO_2$/graphite systems. Therefore, one can conclude that the polymerization mechanism of VC at the surface of the graphite electrode does not require the presence of the $LiCoO_2$ electrode.

F 1s and P 2p core peaks: To complete the XPS characterization of the SEI on the graphite electrode, F 1s and P 2p core peaks have been also analyzed. Since no clear evolution was observed upon discharge whether VC is present as additive or not, only the spectra of the sample discharged at 0.01 V using the VC-containing electrolyte have been displayed in Figure 4 as a representative example. The F 1s spectrum shows two peaks. The first one at 687 eV is attributed to the remaining salt $LiPF_6$, despite washing the electrode with DMC before XPS analysis. The second one at 685.1 eV is attributed to LiF, which is a degradation product of $LiPF_6$ commonly observed at electrode/electrolyte interfaces. The P 2p spectrum shows two components (which are asymmetric because they include $2p_{3/2}$ and $2p_{1/2}$ separated by ~0.9 eV). The first one at 137 eV is attributed to the remaining $LiPF_6$. The other one at

134.4 can be assigned to phosphates that result from degradation of $LiPF_6$. Several mechanisms have been proposed to explain the formation of these species [6,40,43], particularly by reaction of $LiPF_6$ with the traces of water in the electrolyte. These reactions are also leading to the formation of LiF. Therefore, the SEI is not only composed of organic species but also of inorganic compounds coming from the degradation of the salt. This phenomenon is also observed with the $LiCoO_2$/graphite system.

3.2. $LiCoO_2/Li_4Ti_5O_{12}$ system:

The second step of this study concerns the $LiCoO_2/Li_4Ti_5O_{12}$ system. In this case, the potential and the chemical nature of the negative electrode are changed with respect to the $LiCoO_2$/graphite system. The electrochemical properties of $Li_4Ti_5O_{12}$ as negative electrode material have been widely studied [44-47], and it is well known to display a very flat plateau at 1.55 V vs. Li^+/Li upon insertion of lithium ions in its tridimensional spinel structure. The voltage obtained with a cell made up of a $LiCoO_2$ positive electrode and a $Li_4Ti_5O_{12}$ negative electrode is of course lower than with a $LiCoO_2$/graphite cell. In our study, the first charge of the $LiCoO_2/Li_4Ti_5O_{12}$ cell was stopped at the following potentials: 2.09, 2.18, 2.34 and 2.65 V in the same experimental conditions: *(a)* with $LiPF_6$ 1mol/L in EC:DEC:DMC as electrolyte (VC-free), and *(b)* with a few percent of VC additive, at 20°C. The samples studied by XPS are highlighted by points in Figure 2.

3.2.1. $LiCoO_2$ positive electrode ($LiCoO_2/Li_4Ti_5O_{12}$):

Figure 5 shows O 1s spectra of the $LiCoO_2$ positive electrodes during the first charge of the battery (C 1s spectra are not shown because they are dominated by PVdF and conductive carbon peaks, because of the great specific surface area of carbon particles and the covering effect of $LiCoO_2$ particles by the PVdF binder at the surface).

The O 1s spectrum of the fresh positive electrode displays the expected shape for $LiCoO_2$. The narrow peak at 529.7 eV is characteristic of O^{2-} anions of the crystalline network. The

second peak at 532 eV is assigned to oxygen anions of $LiCoO_2$ of the surface, which have a deficient coordination, and also to a weak contamination of absorbed species at the surface [48].

Upon charge, for both series of samples we can observe the appearance of new peaks, showing the formation of a passivating film at the surface of the $LiCoO_2$ electrode. When the VC-free electrolyte is used (series *a*), two new peaks appear at 531.8 and 533.6 eV. This is in good agreement with the deposition of carbonate salts (Li_2CO_3 and/or lithium alkyl carbonates $ROCO_2Li$), resulting from the decomposition of the solvents EC, DEC and DMC, as observed previously for the composite graphite electrode. An accurate attribution of these components is however difficult here because C 1s spectra are not exploitable.

When VC is added in the electrolyte (series *b*), two new O 1s components at ~533 and 534.5 eV appear and their intensities increase upon charge. This particular signature at high binding energy (534.5 eV) shows that the VC polymer is present at the surface of the $LiCoO_2$ electrode. The overall evolution is rather close to that observed for the $LiCoO_2$/graphite system (described in ref. [35], and partially shown in figure 1*b*). The only difference is that the surface layer is thinner here, because the intensity of the characteristic O 1s peak of $LiCoO_2$ does not significantly decrease. These results show that the same VC degradation mechanism is observed at the surface of $LiCoO_2$ whether a graphite or a $Li_4Ti_5O_{12}$ negative electrode is used.

3.2.2. $Li_4Ti_5O_{12}$ negative electrode ($LiCoO_2$/$Li_4Ti_5O_{12}$):

Figure 6 shows Ti 2p, Ti 3s and Li 1s spectra of the $Li_4Ti_5O_{12}$ negative electrode during the first charge of the $LiCoO_2$/$Li_4Ti_5O_{12}$ cell. Since no difference was observed upon charge whether VC is present as additive or not, only one series of spectra has been shown as an example (without VC).

The Ti 2p core peak of the fresh $Li_4Ti_5O_{12}$ electrode is split in two parts due to spin-orbit

coupling, with an area ratio of about 2/1. The Ti $2p_{3/2}$ component is observed at 458.8 eV and Ti $2p_{1/2}$ at 464.6 eV, in good agreement with Ti^{4+} ions in an oxygen environment. Upon charge of the $LiCoO_2/Li_4Ti_5O_{12}$ cell (especially at 2.34 and 2.65 V), we can observe the replacement of the Ti $2p_{3/2}$ peak at 458.8 eV by a new one at 456.9 eV (characteristic of Ti^{3+}). The same observation can be made for the Ti $2p_{1/2}$ component. This is an experimental evidence of the reduction process of Ti^{4+} into Ti^{3+} accompanying the insertion of lithium ions into $Li_4Ti_5O_{12}$. Figure 6*b* shows Ti 3s and Li 1s core peaks of the $Li_4Ti_5O_{12}$ electrode in the same binding energy region (the intensity difference is due to XPS cross-sections). Upon charge, we can observe the increase of an additional Li 1s component at 55.7 eV, which corresponds to lithiated compounds deposited at the surface of the electrode.

Figure 7 shows O 1s spectra of the $Li_4Ti_5O_{12}$ negative electrode upon the first charge of the $LiCoO_2/Li_4Ti_5O_{12}$ cell: *(a)* with $LiPF_6$ 1mol/L in EC:DEC:DMC as electrolyte (VC-free), and *(b)* with a few percent of VC additive (C 1s spectra are not shown because of PVdF, as said above).

The O 1s spectrum of the fresh electrode consists of two peaks. The narrow peak at 530.2 eV is assigned to oxygen atoms of the $Li_4Ti_5O_{12}$ lattice. The smaller peak at 532.2 eV is probably associated to adsorbed oxygenated species. Upon charge, for both series of samples, we can observe a decrease of the $Li_4Ti_5O_{12}$ peak at 530.2 eV, and the appearance of new components at 532 and 533-534 eV. These binding energy values and the observed intensity ratio are in good agreement with the deposition of carbonate salts (Li_2CO_3 and/or $ROCO_2Li$), resulting from the decomposition of the solvents EC, DEC and DMC at the surface of the $Li_4Ti_5O_{12}$ electrode. In the same time, F 1s spectra reveal the deposition of a small amount of LiF (not shown here). The deposition of carbonate compounds and LiF are also consistent with the appearance of the new Li 1s peak at 55.7 eV, as shown in figure 6*b*. This is an interesting result, because $Li_4Ti_5O_{12}$ is usually considered as a passivation-free electrode

material. Indeed, because the main reduction processes of the solvents occur at potentials lower than 0.8 V vs. Li^+/Li, a SEI film formation is not expected to occur on this 1.55 V electrode, and it is actually not detected by electrochemical cycling or AC impedance measurements [49-52]. However, deposited species can be detected by XPS at the surface of this electrode. Other mechanisms than the electrochemical reduction of the solvents at the negative electrode surface have thus to be considered to explain the formation of these species.

An important point to notice is that the overall evolution is the same for both series of samples, and that the same peaks are observed whether VC is present as additive or not. Especially, the characteristic signature of the VC polymer at 534.5 eV is not observed at the $Li_4Ti_5O_{12}$ electrode/electrolyte interface when VC is present as additive, even at the end of charge (2.65 V). This is certainly due to the 1.55 V potential of the $Li_4Ti_5O_{12}$ electrode, which is too high to observe the reduction of VC. This result shows that the particular VC polymerization mechanism observed at the surface of the graphite electrode in a $LiCoO_2$/graphite cell [35] is not observed at the surface of the $Li_4Ti_5O_{12}$ electrode in a $LiCoO_2/Li_4Ti_5O_{12}$ cell, whereas simultaneously the same mechanism is observed at the surface of the $LiCoO_2$ positive electrode for both systems. This is a second important result: it shows that the VC polymerization mechanism can occur at the surface of the positive electrode independently of the negative one. Therefore, it can also be linked to the high potential of the positive electrode upon charge, and thus to oxidation processes.

3.3. $LiFePO_4$/graphite system:

The third step of this study concerns the $LiFePO_4$/graphite system. In this case, the potential and the chemical nature of the positive electrode are changed with respect to the $LiCoO_2$/graphite system. $LiFePO_4$ was shown to be a very interesting positive electrode material for Li-ion batteries because of its safety and its ability to be used at very high cycling

rates, which makes it one of the most promising positive electrode materials for electric and hybrid vehicles applications [53-57]. Many studies have been devoted to optimizing the synthesis conditions of this material, to improve its electrochemical performances and to understand the lithium intercalation/deintercalation mechanisms [58-66].

$LiFePO_4$ displays a voltage plateau at about 3.5 V vs. Li^+/Li. In our study, the first charge of the $LiFePO_4$/graphite cell was stopped at the following potentials: 1.8, 2.8, 3.4 and 4.5 V in the same experimental conditions: *(a)* with $LiPF_6$ 1mol/L in EC:DEC:DMC as electrolyte (VC-free), and *(b)* with a few percent of VC additive, at 20°C. The samples studied by XPS are highlighted by points in Figure 2.

3.3.1. $LiFePO_4$ positive electrode ($LiFePO_4$/graphite):

Figure 8 shows Fe 2p and P 2p spectra of the $LiFePO_4$ positive electrode upon the first charge of the $LiFePO_4$/graphite cell. Since no difference was observed upon charge whether VC is present as additive or not, only one series of spectra has been shown (without VC).

Fe 2p core peak: The Fe 2p spectrum of the fresh $LiFePO_4$ electrode is split in two parts due to spin-orbit coupling (Fe $2p_{3/2}$ and Fe $2p_{1/2}$) with an intensity ratio of about 2/1. Each part consists of a main peak and a "shake-up" satellite [67]. $LiFePO_4$ shows a Fe $2p_{3/2}$ main peak at 710 eV with a satellite peak at ~715 eV. The spectrum of the fresh electrode is in good agreement with Fe^{2+} ions in an oxygen environment. The fine structure of the Fe $2p_{3/2}$ main peak (at 709.5 and 710.5 eV) can be explained by a multiplet effect [66].

Upon charge, we can observe a gradual decrease of the Fe $2p_{3/2}$ main peak at 710 eV (characteristic of Fe^{2+}), and a gradual enhancement of a new peak at 712 eV (characteristic of Fe^{3+}). The same evolution can be also clearly observed for the Fe $2p_{1/2}$ peak, showing the two-phase reaction between $LiFePO_4$ and $FePO_4$ following lithium deintercalation.

P 2p core peak: The P 2p spectrum of the fresh $LiFePO_4$ electrode consists of one asymmetric doublet at 133.5 eV (including $2p_{3/2}$-$2p_{1/2}$ components separated by ~0.9 eV; only

the envelope has been represented). The presence of only one P 2p doublet at this binding energy reveals the presence of only one environment for phosphorus, in good agreement with a $(PO_4)^{3-}$ phosphate group.

Upon charge, we can observe the appearance of two additional doublets at ~134.2 and ~135.5 eV. They can be assigned to a weak amount of phosphates and fluorophosphates compounds, respectively, that result from degradation of the salt $LiPF_6$. Simultaneously, a weak amount of LiF can be detected in F 1s spectra (not shown). Note that C 1s spectra are not shown here because they are dominated by PVdF, which is also the binder used in this electrode.

O 1s core peak: Figure 9 shows the O 1s spectra of the $LiFePO_4$ positive electrode during the first charge of the battery: *(a)* with the VC-free electrolyte, and *(b)* with addition of VC. The spectrum of the fresh electrode displays a narrow peak at 531.4 eV which is attributed to oxygen atoms of $(PO_4)^{3-}$ phosphate groups. We can also notice a weak component at 533 eV which is assigned to contaminating species adsorbed at the surface.

Upon charge, for both series of samples we can first notice that the characteristic peak of $LiFePO_4$ at 531.4 eV still remains the main peak of the O 1s spectrum. A slight increase of the O 1s component at 533 eV can be observed, showing the deposition of a small amount of oxygenated species ensuing from electrolyte degradation. However, the passivating film remains very thin at the end of charge, which is in good agreement with a previous work showing that the surface of the $LiFePO_4$ particles is not very reactive toward the electrolyte upon charge [66]. The most important point to notice here is that no difference in the O 1s spectra is observed whether VC is present as additive or not. Indeed, the characteristic signature of the VC polymer at 534.5 eV is not observed at the $LiFePO_4$ electrode/electrolyte interface when VC is present as additive, in spite of the high voltage value reached at the end of charge (4.5 V). Therefore, the particular VC polymerization mechanism observed at the

surface of the $LiCoO_2$ electrode in a $LiCoO_2$/graphite cell does not occur at the surface of the $LiFePO_4$ electrode in a $LiFePO_4$/graphite cell.

In parallel, P 2p and F 1s spectra reveal the deposition of a small amount of LiF and phosphates and fluorophosphates (not shown).

3.3.2. Graphite negative electrode ($LiFePO_4$/graphite):

Figure 10 shows C 1s and O 1s spectra of the graphite negative electrode of the same cells: *(a)* with the VC-free electrolyte, *(b)* with VC added.

C 1s core peak: The overall evolution of C 1s spectra upon charge of $LiFePO_4$/graphite cells can be compared to that observed previously in figure 3 for the graphite electrode upon discharge of the graphite/Li half-cells. For both series of samples, we can observe the same decrease of the graphite component at 284.3 eV, showing that the graphite surface has been covered by a SEI film. The C 1s spectra obtained at 3.4 and 4.5 V are rather similar to those obtained at the end of discharge for the graphite/Li half-cells. The same way, new peaks attributed to carbonate species can be observed at 290-290.5 eV, resulting from the decomposition of the solvents EC, DEC and DMC. An additional weak peak at 291.3 eV is even hardly detectable at the end of charge with the VC-containing electrolyte. As a result, a similar evolution of the graphite electrode/electrolyte interface is observed as in the case of $LiCoO_2$/graphite and graphite/Li systems.

O 1s core peak: For both series of samples, we can also observe the same overall evolution of O 1s spectra as in the case of graphite/Li half-cells. Indeed, after charge at 3.4 and 4.5 V the spectra are very different whether VC is present as additive or not. Particularly, the characteristic signature of the VC polymer at 534.5 eV is clearly observed with the VC-containing electrolyte. As a summary, this result shows that the same particular VC polymerization mechanism is observed at the surface of the graphite electrode in both $LiCoO_2$/graphite and $LiFePO_4$/graphite systems. However, simultaneously the VC

polymerization mechanism is not observed at the surface of the $LiFePO_4$ electrode. This is in good agreement with the conclusions of the study of the graphite/Li system, showing that this VC polymerization mechanism can occur at the negative electrode independently of the positive electrode. However, this result also shows that both positive electrode materials have a different reactivity towards the electrolyte. The potential of the electrode during Li^+ deintercalation can not be put forward, because the final voltage of the $LiFePO_4$/graphite cell is 4.5 V, even higher than that of the $LiCoO_2$/graphite cell (4.2 V). Therefore, another explanation has to be found. This result leads us to conclude that the chemical nature of the positive electrode also plays an important role in the electrolyte degradation mechanisms at its surface. It was already shown that the surface film covering a $LiFePO_4$ electrode is much thinner than that covering a $LiCoO_2$ electrode at the end of charge [66]. Therefore, the surface of $LiCoO_2$ may have a specific reactivity that participates to surface film formation.

3.4. Electrochemical results:

Figure 11 shows the differential capacity *dQ/dV* vs. voltage V plots obtained for $LiCoO_2$/graphite, graphite/Li and $LiCoO_2/Li_4Ti_5O_{12}$ systems, with and without VC additive in the electrolyte. These *dQ/dV* plots correspond to the galvanostatic charge (or discharge for C/Li) curves presented in Figure 2. For each system they show the voltage window of the beginning of charge (discharge), *i.e.* before lithium intercalation/deintercalation occurs in the active electrode materials, in order to better evidence the electrochemical processes involved by electrolyte degradation.

Figure 11*a* shows the *dQ/dV* plot of the $LiCoO_2$/graphite cell. First, we can notice two shoulders at 3.0 and 3.2 V which are observed whether VC is present as additive or not. These peaks can thus be assigned to electrochemical processes that do not involve VC, *i.e.* reduction of the other solvents EC, DEC or DMC at the negative electrode surface (3.0 and 3.2 V correspond to ~0.8 and 0.6 V vs. Li^+/Li for the graphite electrode potential, respectively). At a

lower cell voltage, an additional weak peak can be observed at ~2.4–2.5 V when VC is added in the electrolyte, as shown in the zoom inset. To confirm the origin of this peak, an additional electrochemical charge was carried out with a $LiCoO_2$/graphite cell using $LiPF_6$ 1 mol/L in pure VC solvent as electrolyte [35]. As the same peak can be observed with a much higher intensity, this result shows that this peak can be unambiguously assigned to the degradation of VC.

Figure 11*b* shows the *dQ/dV* plot of the graphite/Li half-cell. In this figure, two peaks at 0.8 and 0.6 V can be observed whether VC is present as additive or not, and are therefore attributed to the reduction of EC, DEC or DMC solvents at the graphite electrode, in good agreement with the results obtained for the $LiCoO_2$/graphite cell. When VC is added in the electrolyte, an additional weak peak can be observed at ~1.25 V, as shown in the zoom inset. This peak can thus be assigned to the reduction of VC, and corresponds to the equivalent peak observed at ~2.4–2.5 V for the $LiCoO_2$/graphite cell. The presence of this reduction peak at 1.25 V vs. Li^+/Li was previously evidenced by Aurbach *et al.* by electrochemical quartz crystal microbalance measurements [29], and illustrates the ability of VC additive to react at a lower battery voltage than the other solvents, and thus to efficiently contribute to the formation of the SEI at the graphite electrode surface. The comparison of *dQ/dV* plots of $LiCoO_2$/graphite and graphite/Li systems is also consistent with XPS results presented above, showing that the VC polymerization product can be detected at the surface of the graphite electrode in both systems.

Figure 11*c* shows the *dQ/dV* plot of the $LiCoO_2/Li_4Ti_5O_{12}$ cell. In this figure, the curve rise observed at ~2.1 V represents the beginning of the lithium intercalation/deintercalation process in the active electrode materials, and no peak corresponding to reduction or oxidation of the solvents or of VC can be detected before this voltage. This is in good agreement with the 1.55 V potential of the $Li_4Ti_5O_{12}$ electrode, since the reduction of VC at the negative

electrode is expected to occur at 1.25 V vs. Li^+/Li and the reduction of the other solvents at a potential lower than 0.8 V. This is also consistent with XPS results showing that the VC polymer is not detected at the surface of this $Li_4Ti_5O_{12}$ electrode. Aside from these results, it was shown by XPS that the VC polymer can be observed at the surface of the $LiCoO_2$ positive electrode independently of the negative one. Therefore, how can we explain that no peak corresponding to an oxidation process at the positive electrode can be detected in the *dQ/dV* plot of the $LiCoO_2/Li_4Ti_5O_{12}$ cell ? Actually it was seen in figure 11*a* and 11*b* that such a peak can be very weak, and so it may be obscured by the high intensity *dQ/dV* peak corresponding to lithium intercalation/deintercalation in the active electrode materials for a cell voltage greater than ~2.1 V (which corresponds to an oxidation potential of VC at the $LiCoO_2$ electrode greater than ~3.7 V vs. Li^+/Li).

Note that the *dQ/dV* plot obtained for the $LiFePO_4$/graphite system could not be analyzed in the same way, because it was disturbed by side peaks at ~2.1–2.3 V cell voltage. Some authors have reported the existence of a low voltage plateau at ~2.6 V vs. Li^+/Li in charge curves of $LiFePO_4$/Li half-cells, due to the presence of impurities in the $LiFePO_4$ material or to its oxidation by air [68,69]. These phenomena could explain the side peaks observed at ~2.1–2.3 V in our curves. For this reason, the *dQ/dV* plot obtained for the $LiFePO_4$/graphite system is not shown here.

Except from this, the electrochemical results are consistent with the XPS analysis of the electrode/electrolyte interfaces. The obtained results are depicted in Figure 12. They can be summarized as follows:

(i) The VC polymerization mechanism is observed at the surface of the graphite electrode, even when it does not occur at the positive electrode,

(ii) This mechanism is not observed at the $Li_4Ti_5O_{12}$ electrode, because its 1.55 V potential is too high,

(iii) The same mechanism is observed at the surface of the $LiCoO_2$ electrode, even when it does not occur at the negative electrode,

(iv) It is not observed at the surface of the $LiFePO_4$ electrode, in spite of the high potential reached at the end of charge (4.5 V).

These results show that an interaction between both electrodes in the VC degradation mechanisms leading to the formation of the passivation films can be excluded. Two independent degradation mechanisms of VC occur at the surface of the positive and the negative electrodes. These mechanisms depend on the potential of the electrode: indeed, the reduction of VC at the negative electrode was shown to occur at ~1.25 V vs. Li^+/Li and it is not observed at the surface of the $Li_4Ti_5O_{12}$ electrode (1.55 V vs. Li^+/Li). However, the potential of the electrode is not the only parameter that controls the occurrence of this degradation process: indeed, the oxidation of VC is always observed at the surface of the $LiCoO_2$ electrode with a 4.2 V potential at the end of charge, whereas it is not observed at the surface of the $LiFePO_4$ electrode with a 4.5 V final potential.

We have shown in our previous work that the same polymer, resulting from the radical polymerization of VC, is deposited at the surface of both electrodes [35]. Two independent mechanisms occurring at each electrode are thus finally leading to the same radical polymerization process. Some authors have already proposed a reduction mechanism of VC into a radical anion at the surface of graphite [36]. This could explain the radical polymerization of VC at the negative electrode. One can thus assume that an equivalent oxidation mechanism of VC into a radical cation occurs at the positive electrode, leading finally to the same radical polymerization process, with a possible catalytic activity of the active material surface. Theoretical calculations would be necessary to investigate and better understand kinetic and thermodynamic aspects of such reactions.

4. CONCLUSION

In this work, we have investigated the formation mechanisms of passivating films at the surface of the electrodes of Li-ion batteries when vinylene carbonate is used as electrolyte additive. We compared $LiCoO_2$/C, $LiCoO_2$/$Li_4Ti_5O_{12}$, $LiFePO_4$/C and C/Li systems, in which the chemical nature and the potential of the electrodes are changed. On the basis of XPS analysis of the electrodes after charge/discharge, complemented by the study of electrochemical curves, we could evidence that an interaction between both electrodes in the VC degradation mechanisms, for example by exchange of chemical species from one electrode to the other one, can be excluded. Separate mechanisms occur at the negative electrode on one hand and at the positive electrode on the other hand, although the same VC polymer is deposited at the surface of both electrodes, which results from a radical polymerization process. The results of this study allow a better understanding of the action of VC as electrolyte additive to improve the properties of the passivating films at the surface of the electrodes, and thus to limit aging processes in Li-ion batteries.

ACKNOWLEDGEMENTS

The authors thank French CNRS (national center for scientific research) and Region Aquitaine for financial support.

REFERENCES

[1] P. B. Balbuena, Y. Wang (ed.), *"Lithium-Ion Batteries: Solid-Electrolyte Interphase"*, Imperial College Press, London (2004)

[2] E. Peled, *J. Electrochem. Soc.* **126**, 2047 (1979)

[3] E. Peled, D. Golodnitsky, G. Ardel, *J. Electrochem. Soc.* **144**, L208 (1997)

[4] D. Aurbach, A. Zaban, Y. Ein-Eli, I. Weissman, O. Chusid, B. Markovsky, M. Levi, E. Levi, A. Schechter, E. Granot, *J. Power Sources* **68**, 91 (1997)

[5] D. Aurbach, *J. Power Sources*, **119-121**, 497 (2003)

[6] A. M. Andersson, D. P. Abraham, R. Haasch, S. MacLaren, J. Liu and K. Amine, *J. Electrochem. Soc.*, **149**, A1358-A1369 (2002)

[7] K. Edström, T. Gustafsson, J. O. Thomas, *Electrochim. Acta*, **50**, 397 (2004)

[8] S. Verdier, L. El Ouatani, R. Dedryvère, F. Bonhomme, P. Biensan, D. Gonbeau, *J. Electrochem. Soc.* **154**, A1088 (2007)

[9] S. S. Zhang, *J. Power Sources*, **162**, 1379-1394 (2006)

[10] K. Xu, *Chem. Rev.* **104**, 4303 (2004)

[11] B. Simon, J.-P. Bœuve, *US Patent 5,626,981* (1997)

[12] S.-K. Jeong, M. Inaba, R. Mogi, Y. Iriyama, T. Abe and Z. Ogumi, *Langmuir* **17,** 8281 (2001)

[13] O. Matsuoka, A. Hiwara, T. Omi, M. Toriida, T. Hayashi, C. Tanaka, Y. Saito, T. Ishida, H. Tan, S. S. Ono and S. Yamamoto, *J. Power Sources*, **108,** 128 (2002)

[14] R. Mogi, M. Inaba, S.-K. Jeong, Y. Iriyama, T. Abe, Z. Ogumi, *J. Electrochem. Soc.* **149**, A1578 (2002)

[15] D. Aurbach, K. Gamolsky, B. Markovsky, Y. Gofer, M. Schmidt, U. Heider, *Electrochim. Acta* **47**, 1423 (2002)

[16] H. Buqa, A. Wursig, J. Vetter, M. E. Spahr, F. Krumeich, P. Novak, *J. Power Sources*, **153**, 385 (2006)

[17] H. Ota, K. Shima, M. Ue and J.-I. Yamaki, *Electrochim. Acta* **49**, 565 (2004)

[18] H. Ota, Y. Sakata, Y. Otake, K. Shima, M. Ue and J.-I. Yamaki, *J. Electrochem. Soc.* **151**, A1778 (2004)

[19] H. Ota, Y. Sakata, A. Inoue, S. Yamaguchi, *J. Electrochem. Soc.* **151**, A1659 (2004)

[20] E.-G. Shim, T.-H. Nam, J.-G. Kim, H.-S. Kim, S.-I. Moon, *J. Power Sources,* **172***,* 901 (2007)

[21] X. Zhang, R. Kostecki, T. J. Richardson, J. K. Pugh, P. N. Ross, Jr., *J. Electrochem. Soc.* **148**, A1341 (2001)

[22] S. S. Zhang, K. Xu, T. R. Jow, *Electrochim. Acta*, **51**, 1636 (2006)

[23] M. Herstedt, H. Rensmo, H. Siegbahn and K. Edström, *Electrochim. Acta,* **49,** 2351 (2004)

[24] M. Herstedt, A. M. Andersson, H. Rensmo, H. Siegbahn and K. Edström, *Electrochim. Acta*, **49**, 4939 (2004)

[25] M. Itagaki, S. Yotsuda, N. Kobari, K. Watanabe, S. Kinoshita and M. Ue, *Electrochim. Acta,* **51,** 1629 (2006)

[26] M. Itagaki, N. Kobari, S. Yotsuda, K. Watanabe, S. Kinoshita and M. Ue, *J. Power Sources*, **135**, 255 (2004)

[27] M. Contestabile, M. Morselli, R. Paraventi, R. J. Neat, *J. Power Sources*, **119-121**, 943 (2003)

[28] T. Sasaki, T. Abe, Y. Iriyama, M. Inaba, Z. Ogumi, *J. Electrochem. Soc.*, **152**, A2046 (2005)

[29] D. Aurbach, B. Markovsky, A. Rodkin, E. Levi, Y. S. Cohen, H.-J. Kim, M. Schmidt, *Electrochim. Acta*, **47**, 4291 (2002)

[30] M. Itagaki, N. Kobari, S. Yotsuda, K. Watanabe, S. Kinoshita, M. Ue, *J. Power Sources* **148**, 78 (2005)

[31] J. Vetter, M. Holzapfel, A. Wuersig, W. Scheifele, J. Ufheil, P. Novak, *J. Power Sources*, **159**, 277 (2006)

[32] M. Holzapfel, A. Wursig, W. Scheifele, J. Vetter and P. Novak, *J. Power Sources*, **174**, 1156 (2007)

[33] H.-C. Wu, C.-Y. Su, D.-T. Shieh, M.-H. Yang, N.-L. Wu, *Electrochem. Solid-State Lett.* **9**, A537 (2006)

[34] M. Holzapfel, C. Jost, A. Prodi-Schwab, F. Krumeich, A. Wursig, H. Buqa, P. Novák, *Carbon* **43**, 1488 (2005)

[35] L. El Ouatani, R. Dedryvère, C. Siret, P. Biensan, S. Reynaud, P. Iratçabal, D. Gonbeau, *J. Electrochem. Soc*, **156**, A103-A113 (2009)

[36] Y. Wang, S. Nakamura, K. Tasaki, P. B. Balbuena, *J. Am. Chem. Soc.*, **124**, 4408-4421 (2002)

[37] D. A. Shirley, *Phys. Rev. B* **5**, 4709 (1972)

[38] J. H. Scofield, *J. Electron Spectrosc. Relat. Phenom.* **8**, 129-137 (1976)

[39] D. Briggs, M. P. Seah, in "*Practical Surface Analysis by Auger and X-ray Photoelectron Spectroscopy"* ; J. Wiley and sons (ed.), D. Briggs (1983)

[40] D. Aurbach, *J. Power Sources* **89**, 206-218 (2000)

[41] S. Laruelle, S. Pilard, P. Guenot, S. Grugeon, J-M. Tarascon, *J. Electrochem. Soc.* **151**, A1202-A1209 (2004)

[42] R. Dedryvère, L. Gireaud, S. Grugeon, S. Laruelle, J-M. Tarascon, D. Gonbeau, *J. Phys. Chem. B* **109**, 15868-15875 (2005)

[43] J. Vetter, P. Novak, M. R. Wagner, C. Veit, K. C. Moller, J. O. Besenhard, M. Winter, M. Wohlfahrt Mehrens, C. Vogler, A. Hammouche, *J. Power Sources*, **147**, 269-281 (2005)

[44] T. Ohzuku, A. Ueda, N. Yamamoto, *J. Electrochem. Soc.* **142**, 1431-1435 (1995)

[45] A. Guerfi, S. Sévigny, M. Lagacé, P. Hovington, K. Kinoshita, K. Zaghib, *J. Power Sources*, **119-121**, 88-94 (2003)

[46] K. Ariyoshi, S. Yamamoto, T. Ohzuku, *J. Power Sources*, **119-121**, 959-963 (2003)

[47] S.-W. Woo, K. Dokko, K. Kanamura, *Electrochim. Acta*, **53**, 79-82 (2007)

[48] L. Dahéron, R. Dedryvère, H. Martinez, M. Ménétrier, C. Delmas, D. Gonbeau, *Chem. Mater.*, **20**, 583-590 (2008)

[49] G. X. Wang, D. H. Bradhurst, S. X. Dou, H. K. Liu, *J. Power Sources*, **83**, 156-161 (1999)

[50] S. Panero, D. Satolli, M. Salomon, B. Scrosati, *Electrochem. Commun.*, **2**, 810-813 (2000)

[51] P. P. Prosini, R. Mancini, L. Petrucci, V. Contini, P. Villano, *Solid State Ionics*, **144**, 185-192 (2001)

[52] D. P. Abraham, E. M. Reynolds, E. Sammann, A. N. Jansen, D. W. Dees, *Electrochim. Acta*, **51**, 502-510 (2005)

[53] A. K. Padhi, K. S. Nanjundaswamy, J. B. Goodenough, *J. Electrochem. Soc.* **144**, 1188 (1997)

[54] K. Amine, J. Liu, I. Belharouak, *Electrochem. Commun.*, **7**, 669-673 (2005)

[55] X. Z. Liao, Z. F. Ma, Y. S. He, X. M. Zhang, L. Wang, Y. Jiang, *J. Electrochem. Soc.*, **152**, A1969-A1973 (2005)

[56] C. Delacourt, P. Poizot, J.-M. Tarascon, C. Masquelier, *Nat. Mater.*, **4**, 254-260 (2005)

[57] J. L. Dodd, R. Yazami, B. Fultz, *Electrochem. Solid State Lett.*, **9**, A151-A155 (2006)

[58] N. Ravet, Y. Chouinard, J. F. Magnan, S. Besner, M. Gauthier, M. Armand *J. Power Sources*, **97-98**, 503-507 (2001)

[59] A. Yamada, S. C. Chung, K. Hinokuma, *J. Electrochem. Soc.*, **148**, A224 (2001)

[60] S. Franger, F. Le Cras, C. Bourbon, H. Rouault, *J. Power Sources*, **119-121**, 252-257 (2003)

[61] S. F. Yang, P. Y. Zavalij, M. S. Whittingham, *Electrochem. Commun.*, **3**, 505-508 (2001)

[62] D. Morgan, A. Van der Ven, G. Ceder, *Electrochem. Solid State Lett.*, **7**, A30-A32 (2004)

[63] M. S. Islam, D. J. Driscoll, C. A. J. Fisher, P. R. Slater, *Chem. Mater.*, **17**, 5085-5092 (2005)

[64] G. Y. Chen, X. Y. Song, T. J. Richardson, *Electrochem. Solid State Lett.*, **9**, A295-A298 (2006)

[65] C. Delmas, M. Maccario, L. Croguennec, F. Le Cras, F. Weill, *Nat. Mater.*, **7**, 665-671 (2008)

[66] R. Dedryvère, M. Maccario, L. Croguennec, F. Le Cras, C. Delmas, D. Gonbeau, *Chem. Mater.*, **20**, 7176-7170 (2008)

[67] S. Hüfner, "Photoelectron spectroscopy; principles and applications" (Springer-Verlag, 1995)

[68] Y. L. Cao, L. H. Yu, T. Li, X. P. Ai, H. X. Yang, *J. Power Sources*, **172**, 913-918 (2007)

[69] X. Xia, Z. Wang, L. Chen, *Electrochem. Commun.*, **10**, 1442-1444 (2008)

Figure captions

Scheme 1 : Poly(VC), polymer ensuing from the radical polymerization of VC at the surface of the electrodes [35].

Figure 1 : O 1s core peaks of both electrodes of a $LiCoO_2$/graphite cell after charge at 20°C in the following conditions : *(a)* with $LiPF_6$/EC:DEC:DMC as electrolyte, *(b)* with addition of VC, *(c)* using $LiPF_6$ in pure VC as electrolyte [35].

Figure 2 : **(a)** Voltage (V) vs. positive electrode capacity *Q* (mAh/g) for $LiCoO_2/Li_4Ti_5O_{12}$ and $LiFePO_4$/graphite systems. **(b)** Voltage (V) vs. graphite electrode capacity *Q* (mAh/g) for a graphite/Li half-cell (C/20 rate, electrolyte $LiPF_6$/EC:DEC:DMC + VC).

Figure 3 : Graphite/Li half cells. C 1s and O 1s core peaks of the graphite electrode upon discharge : *(a)* with $LiPF_6$/EC:DEC:DMC electrolyte (VC-free), *(b)* with addition of VC.

Figure 4: Graphite/Li system. F 1s and P 2p core peaks of the graphite electrode after discharge at 0.01 V at 20°C.

Figure 5 : $LiCoO_2/Li_4Ti_5O_{12}$ system : O 1s core peaks of the $LiCoO_2$ electrode upon charge: *(a)* with $LiPF_6$/EC:DEC:DMC electrolyte (VC-free), *(b)* with addition of VC.

Figure 6 : $LiCoO_2/Li_4Ti_5O_{12}$ system. Ti 2p, Ti 3s and Li 1s core peaks of the $Li_4Ti_5O_{12}$ electrode upon charge.

Figure 7 : $LiCoO_2/Li_4Ti_5O_{12}$ system. O 1s core peaks of the $Li_4Ti_5O_{12}$ electrode upon charge : *(a)* with $LiPF_6$/EC:DEC:DMC electrolyte (VC-free), *(b)* with addition of VC.

Figure 8: $LiFePO_4$/graphite system: Fe 2p and P 2p core peaks of the $LiFePO_4$ electrode upon charge.

Figure 9: $LiFePO_4$/graphite system. O 1s core peaks of the $LiFePO_4$ electrode upon charge : *(a)* with $LiPF_6$/EC:DEC:DMC electrolyte (VC-free), *(b)* with addition of VC.

Figure 10 : $LiFePO_4$/graphite system. C 1s and O 1s core peaks of the graphite electrode upon charge : *(a)* with $LiPF_6$/EC:DEC:DMC electrolyte (VC-free), *(b)* with addition of VC.

Figure 11 : Differential capacity dQ/dV ($mAh.g^{-1}.V^{-1}$) upon galvanostatic charge (discharge) at 20°C of : *(a)* $LiCoO_2$/graphite, *(b)* graphite/Li, *(c)* $LiCoO_2/Li_4Ti_5O_{12}$ systems. *Q* is the specific capacity (mAh/g) of the positive electrode (of the graphite electrode for graphite/Li).

Figure 12: Schematic summary of the observed VC degradation mechanisms in the different systems as a function of the electrode nature and voltage.

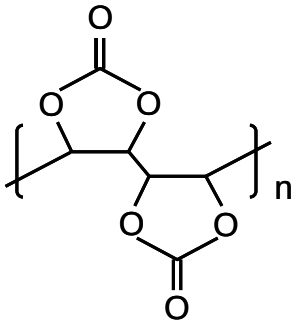

Scheme 1 : Poly(VC), polymer ensuing from the radical polymerization of VC at the surface of the electrodes [35].

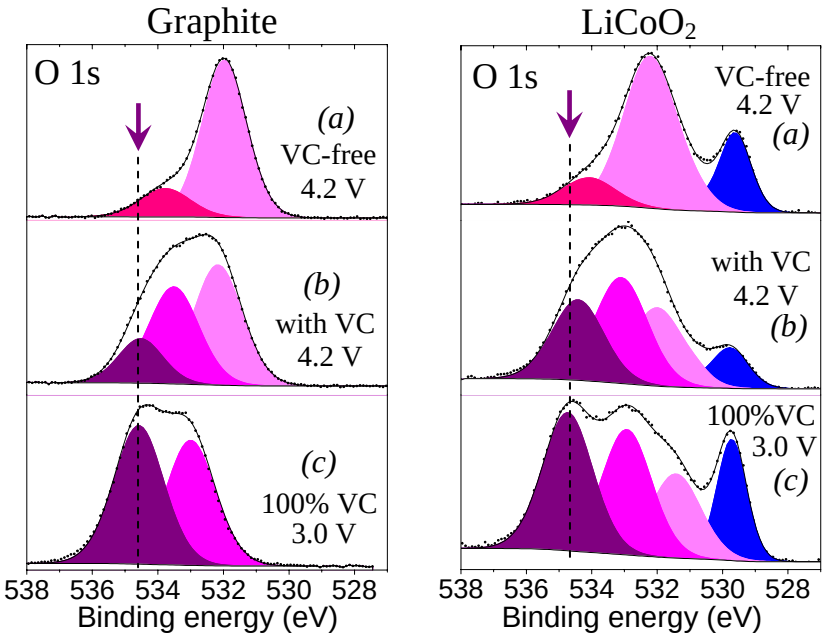

Figure 1 : O 1s core peaks of both electrodes of a $LiCoO_2$/graphite cell after charge at 20°C in the following conditions : *(a)* with $LiPF_6$/EC:DEC:DMC as electrolyte, *(b)* with addition of VC, *(c)* using $LiPF_6$ in pure VC as electrolyte [35].

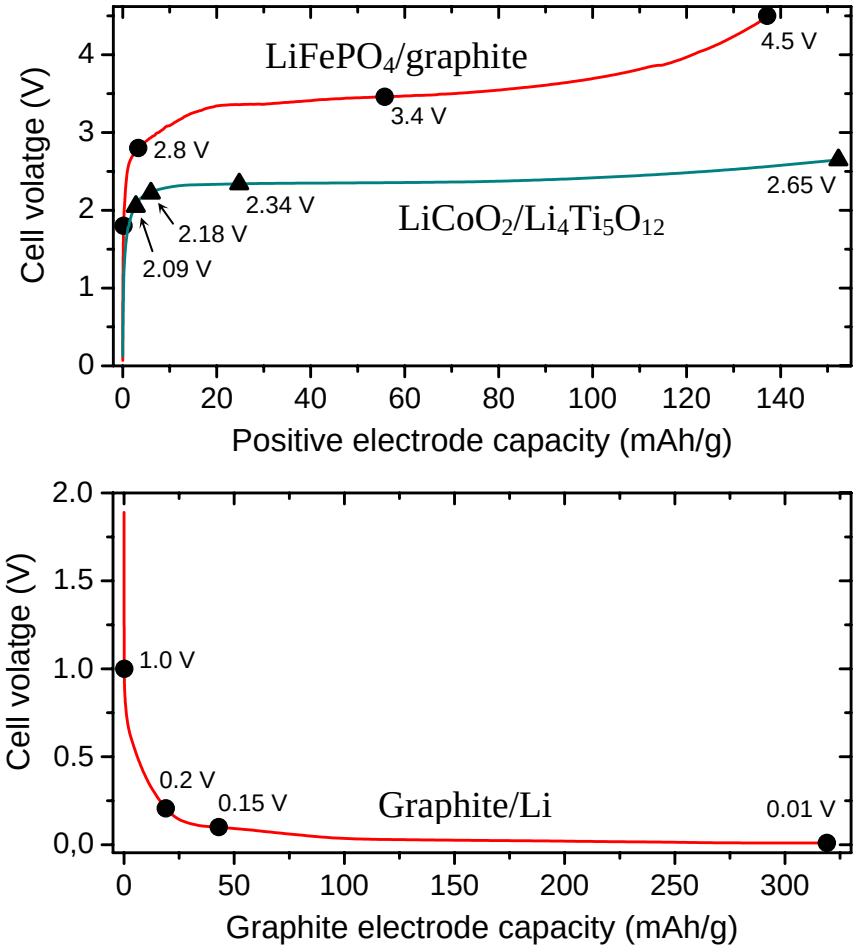

Figure 2 : **(a)** Voltage (V) vs. positive electrode capacity *Q* (mAh/g) for $LiCoO_2/Li_4Ti_5O_{12}$ and $LiFePO_4$/graphite systems. **(b)** Voltage (V) vs. graphite electrode capacity *Q* (mAh/g) for a graphite/Li half-cell (C/20 rate, electrolyte $LiPF_6$/EC:DEC:DMC + VC).

Graphite/Li : graphite electrode

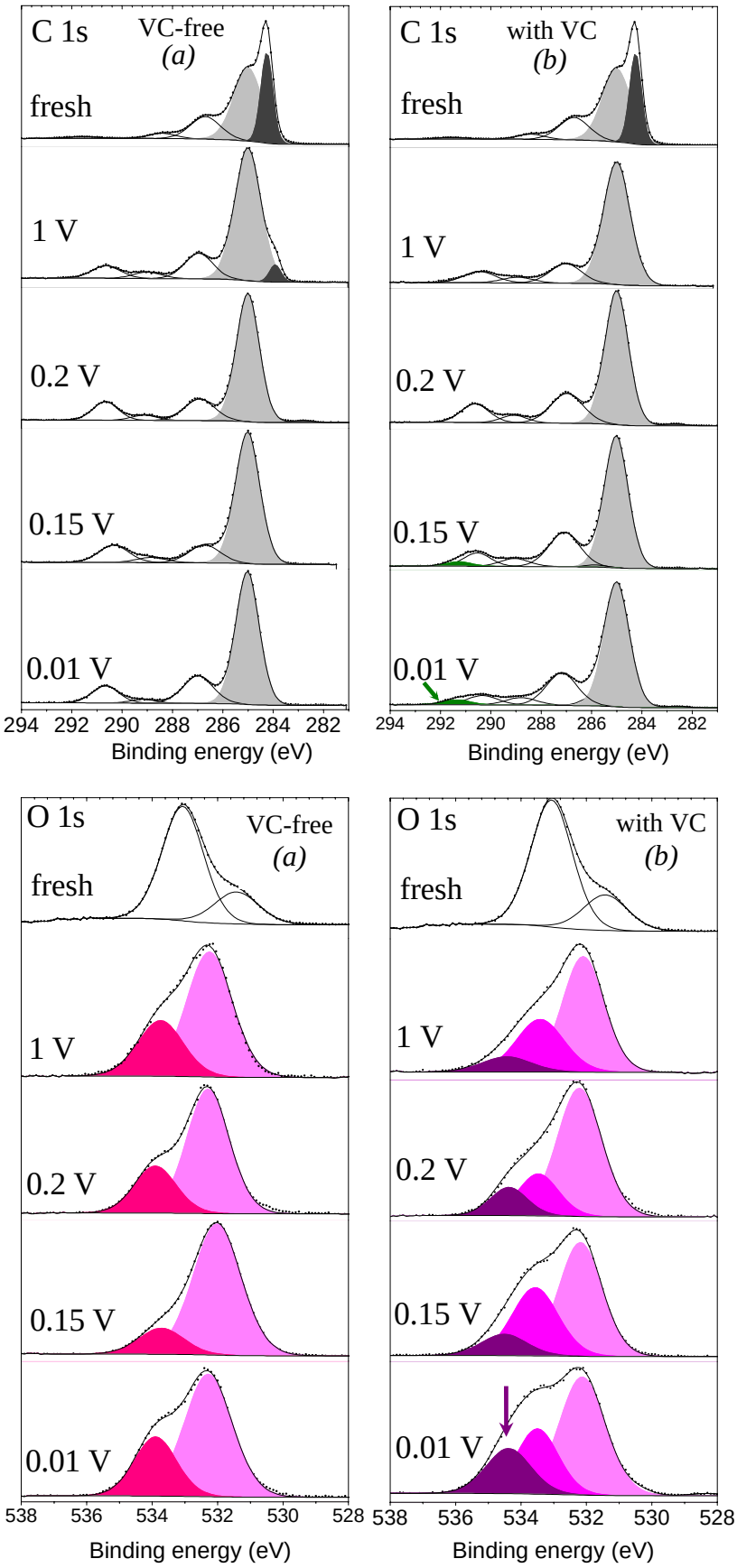

Figure 3 : Graphite/Li half cells. C 1s and O 1s core peaks of the graphite electrode upon discharge : *(a)* with $LiPF_6$/EC:DEC:DMC electrolyte (VC-free), *(b)* with addition of VC.

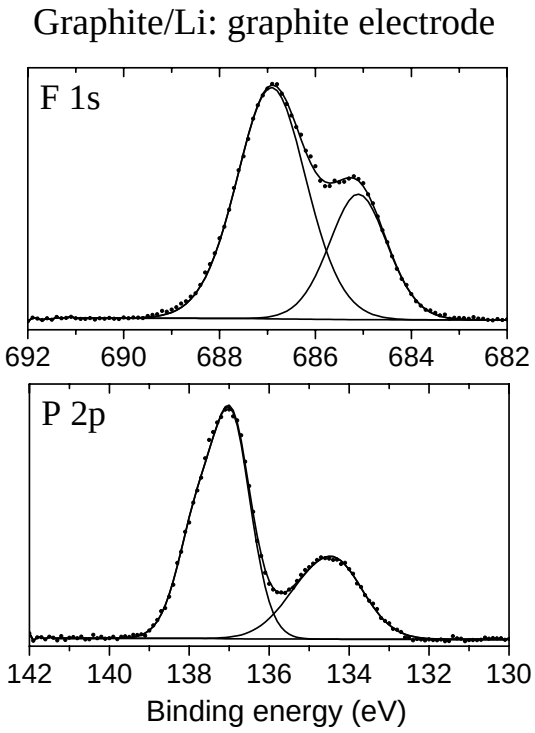

Figure 4: Graphite/Li system. F 1s and P 2p core peaks of the graphite electrode after discharge at 0.01 V at 20°C.

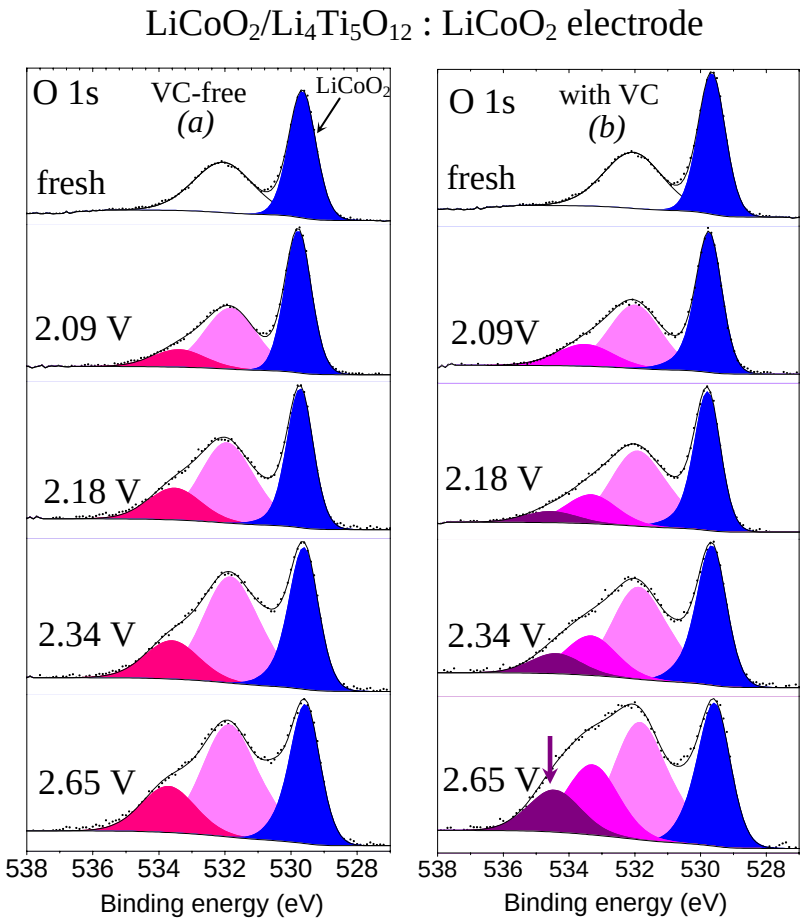

Figure 5 : $LiCoO_2/Li_4Ti_5O_{12}$ system : O 1s core peaks of the $LiCoO_2$ electrode upon charge: *(a)* with $LiPF_6$/EC:DEC:DMC electrolyte (VC-free), *(b)* with addition of VC.

$LiCoO_2/Li_4Ti_5O_{12}$: $Li_4Ti_5O_{12}$ electrode

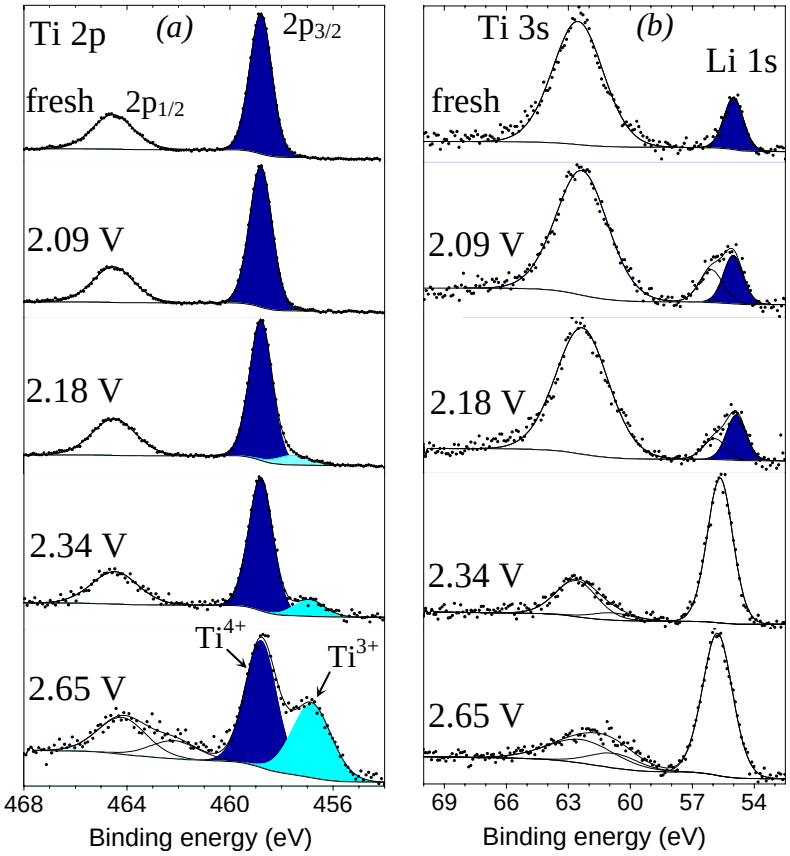

Figure 6 : $LiCoO_2/Li_4Ti_5O_{12}$ system. Ti 2p, Ti 3s and Li 1s core peaks of the $Li_4Ti_5O_{12}$ electrode upon charge.

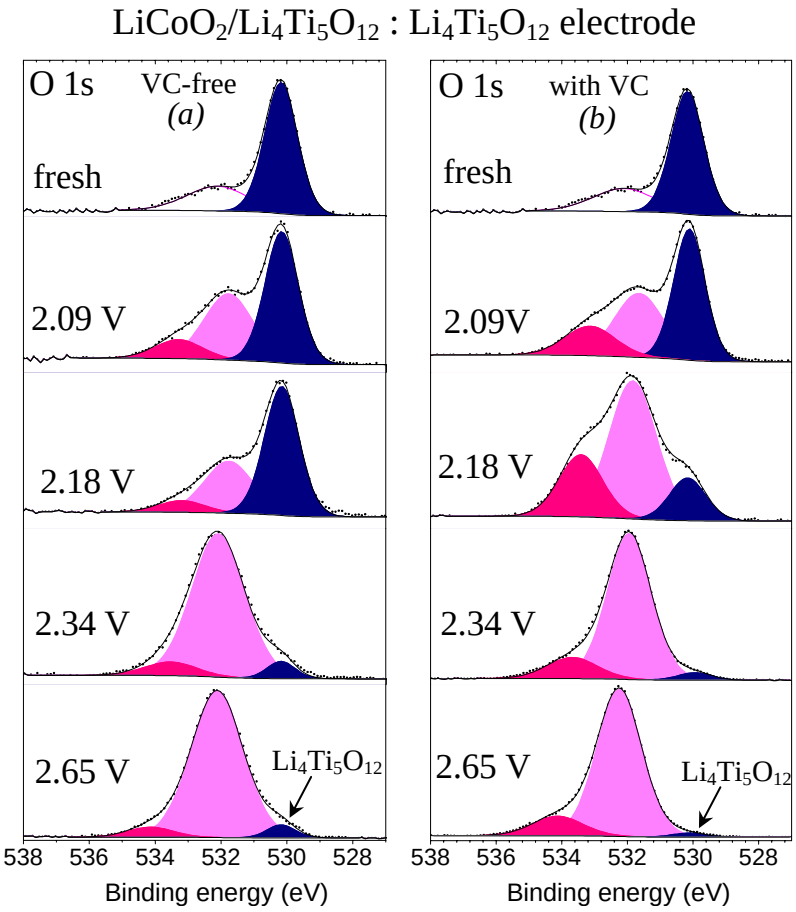

Figure 7 : $LiCoO_2/Li_4Ti_5O_{12}$ system. O 1s core peaks of the $Li_4Ti_5O_{12}$ electrode upon charge : *(a)* with $LiPF_6$/EC:DEC:DMC electrolyte (VC-free), *(b)* with addition of VC.

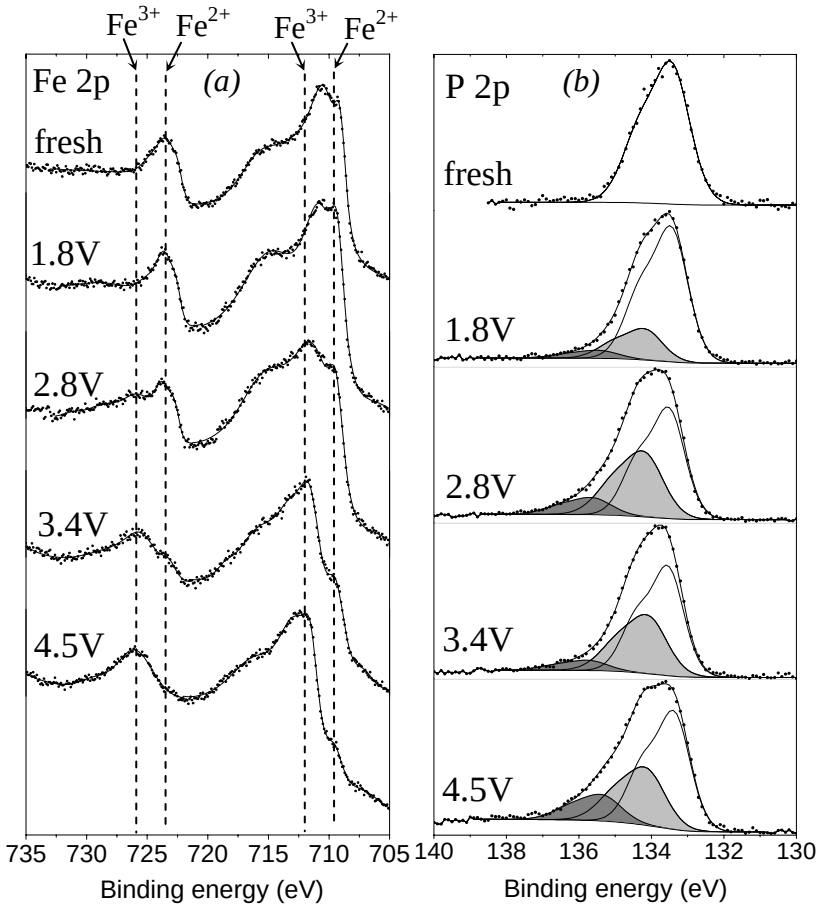

Figure 8: $LiFePO_4$/graphite system: Fe 2p and P 2p core peaks of the $LiFePO_4$ electrode upon charge.

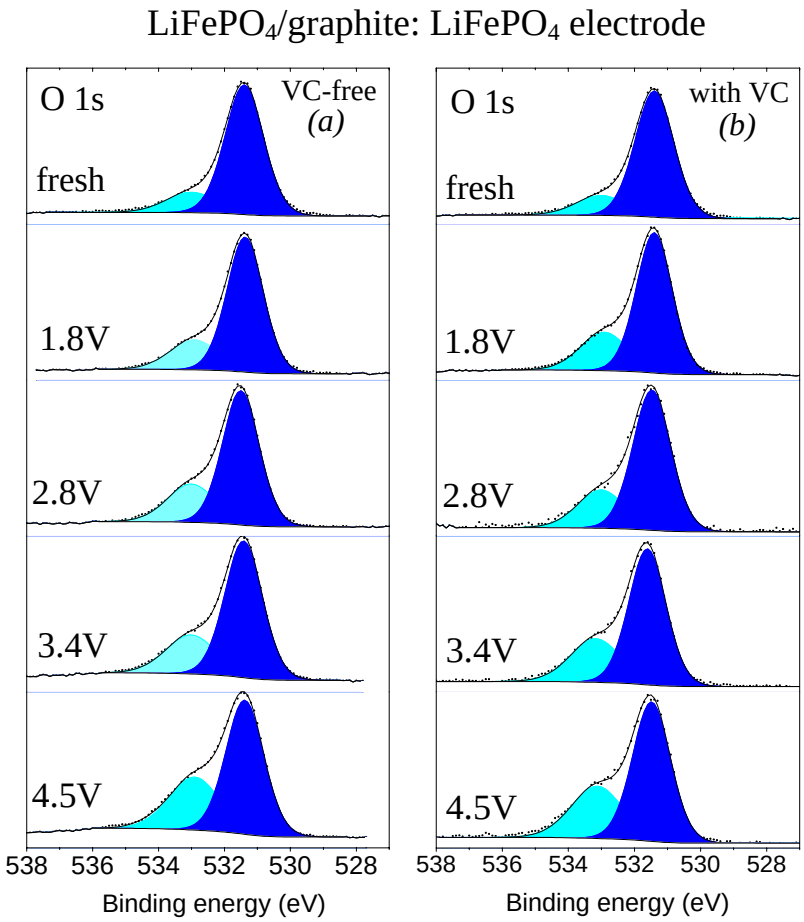

Figure 9: $LiFePO_4$/graphite system. O 1s core peaks of the $LiFePO_4$ electrode upon charge : *(a)* with $LiPF_6$/EC:DEC:DMC electrolyte (VC-free), *(b)* with addition of VC.

LiFePO$_4$/graphite : graphite electrode

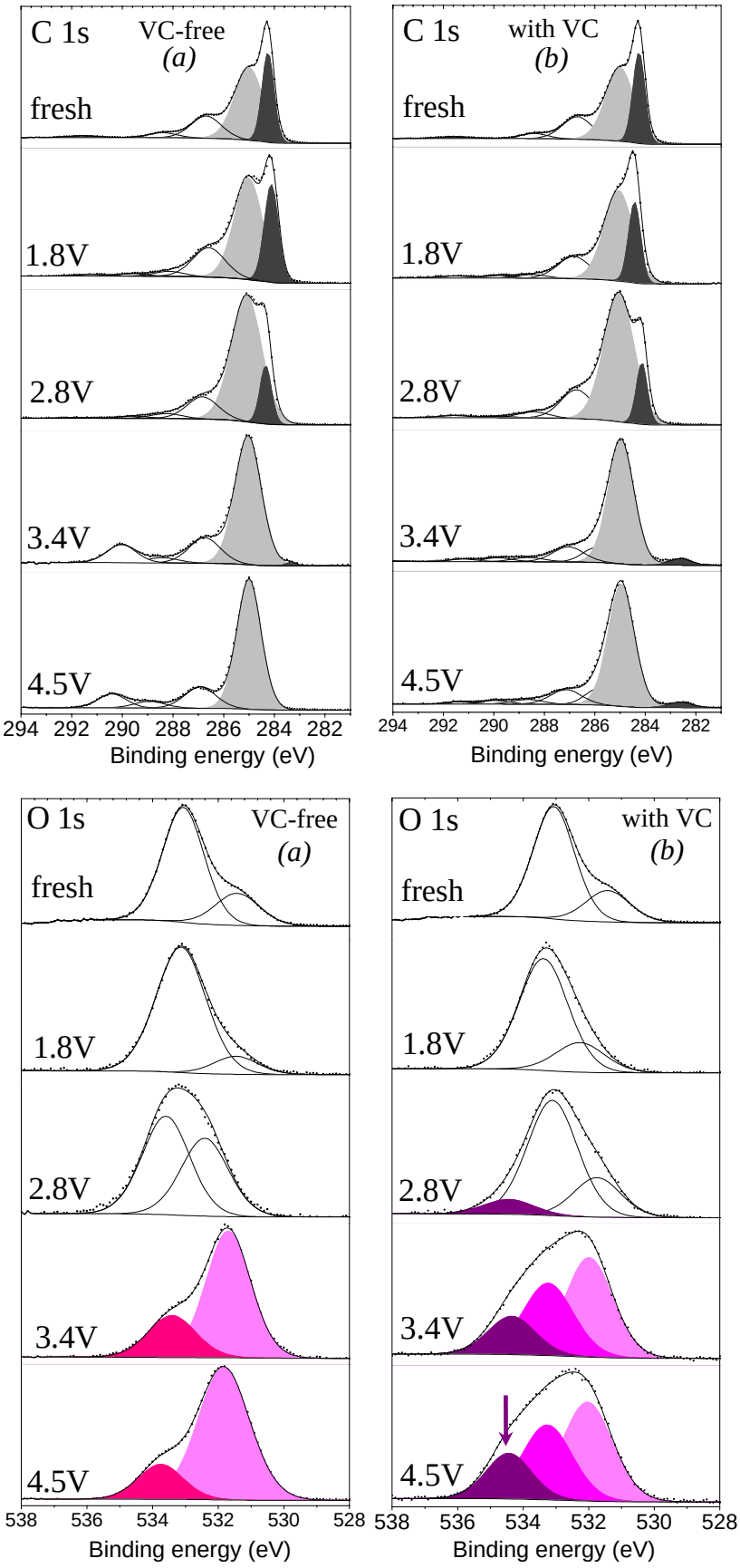

Figure 10 : LiFePO$_4$/graphite system. C 1s and O 1s core peaks of the graphite electrode upon charge : *(a)* with LiPF$_6$/EC:DEC:DMC electrolyte (VC-free), *(b)* with addition of VC.

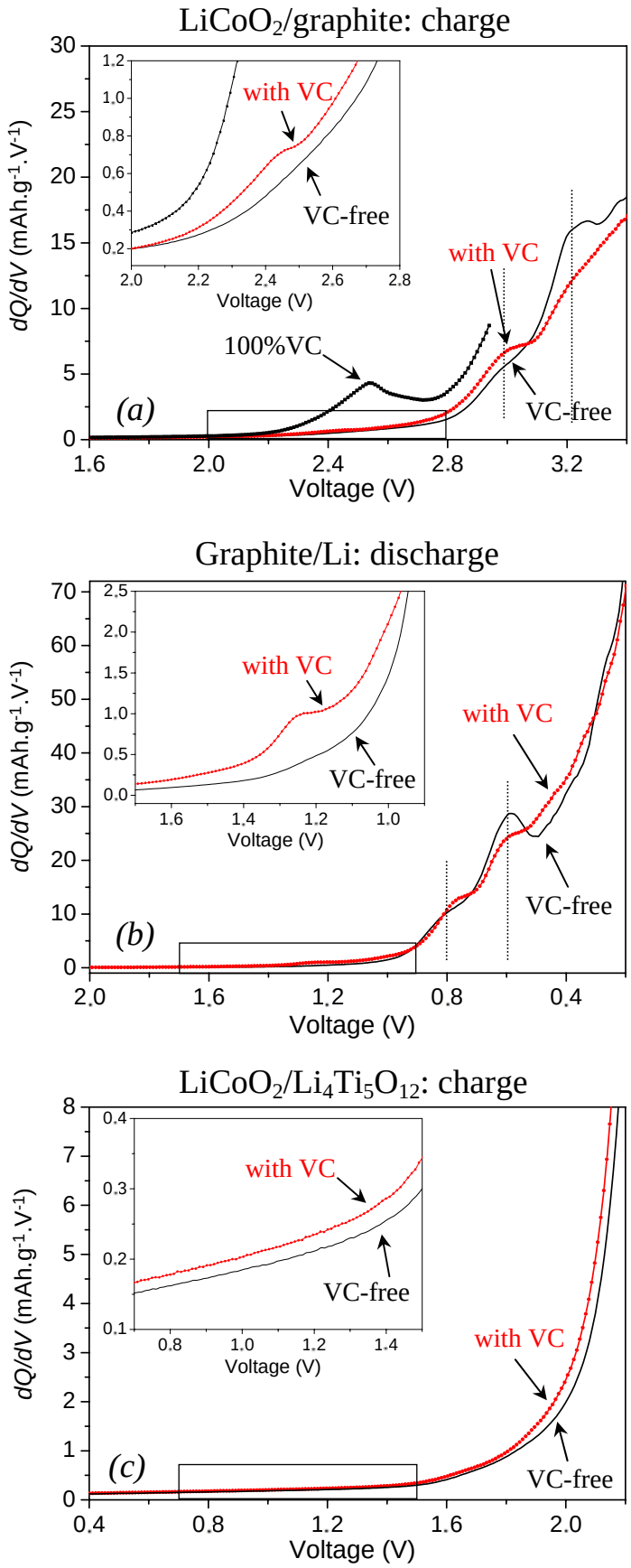

Figure 11 : Differential capacity *dQ/dV* (mAh.g^{-1}.V^{-1}) upon galvanostatic charge (discharge) at 20°C of : *(a)* $LiCoO_2$/graphite, *(b)* graphite/Li, *(c)* $LiCoO_2/Li_4Ti_5O_{12}$ systems. *Q* is the specific capacity (mAh/g) of the positive electrode (of the graphite electrode for graphite/Li).

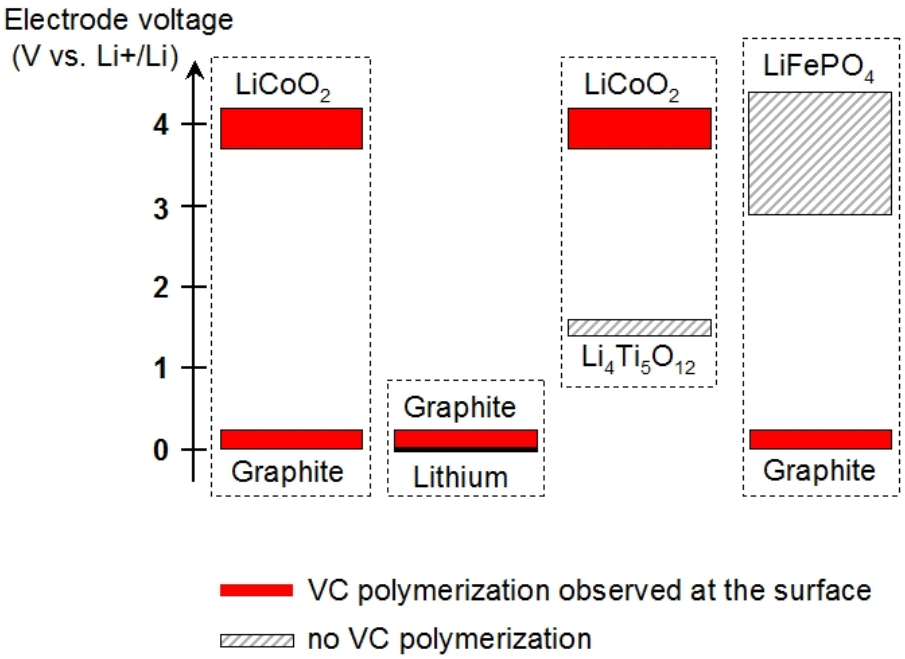

Figure 12: Schematic summary of the observed VC degradation mechanisms in the different systems as a function of the electrode nature and voltage.